Fall 1-24-2013

Effects of Molecular Structure of the Oxidation Products of Reactive Atmospheric Hydrocarbons on the Formation of Secondary Organic Particulate Matter, Including the Effects of Water

Negar Niakan
Portland State University

Effects of Molecular Structure of the Oxidation Products of Reactive Atmospheric Hydrocarbons on the Formation of Secondary Organic Particular Matter, Including the Effects of Water

by

Negar Niakan

A thesis submitted in partial fulfillment of the
requirements for the degree of

Master of Science
in
Civil and Environmental Engineering

Thesis Committee:
James F. Pankow, Chair
William Fish
Kelley C. Barsanti

Portland State University
2012

Abstract

Organic aerosols have significant effects on human health, air quality and climate. Secondary organic aerosols (SOA) are produced by the oxidation of primary-volatile organic compounds (VOC). For example, α-pinene reacts with oxidants such as hydroxyl radical (OH), ozone (O_3), and nitrate radical (NO_3), accounting for a significant portion of total organic aerosol in the atmosphere. Experimental studies have shown that the oxidation process between α-pinene and ozone has the most significant impact in the formation of SOA (Hoffmann *et al.*, 1997). Most of the models used to predict SOA formation, however, are limited in that they neglect the role of water due to uncertainty about the structure and nature of organic compounds, in addition to uncertainty about the effect of varying relative humidity (RH) on atmospheric organic particulate matter (OPM) (Kanakidou *et al.*, 2005). For this study, structures of organic compounds involved in the formation of SOA are estimated, and the role of water uptake is incorporated in the process. The Combinatorial Aerosol Formation Model (CAFM) is a deterministic model used to determine the amount of organic mass (M_o μg m^{-3}) formation based on the predicted structures. Results show that the amount of SOA that is formed is almost negligible when the amount of parent hydrocarbon involved in the reaction is low (*i.e.* around 5 μg m^{-3}), especially at lower RH. Observing compounds with a greater number of polar groups (alcohol and carboxylic acid) indicates that structure has a significant effect on organic mass formation. This observation is in agreement with the fact that the more hydrophilic the compound is, the higher RH, leading to more condensation into the PM phase.

Dedication

My thanks and appreciation to Dr. James F. Pankow for persevering with me as my advisor throughout the time it took me to complete this research and write the dissertation.

I also want to express my gratitude to Dr. William Asher who helped me with the programming and coding for this endeavor.

I also want to thank my family because of all the wonderful things they do for me and supporting me all the way.

Acknowledgements

This work was supported by the Electric Power Research Institute (EPRI).

Table of Contents

List of Tables

Table Number

List of Figures

Figure Number

1. Introduction

1.1. Organic Aerosols and their Effects

Atmospheric aerosol particles in the atmosphere can affect the radiative balance of the Earth by absorbing and scattering solar radiation. Some aerosol particles contain highly absorptive "black carbon", and can raise the air temperature; aerosol particles can also have cooling effects. Particle size has a significant role in determining the effects of atmospheric aerosol particles. Fine particles that have wavelengths similar to light in the visible region are believed to have a higher impact on climate than larger particles (Kanakidou *et al*., 2005), as they can be transported far from their emission sources. In addition, fine particles can have an indirect effect on climate by serving as nuclei for cloud formation. Fine aerosol particles are typically 20-50% organic in composition, and much research has been conducted on their nature and sources. There are two main classes of organic aerosol particles, namely primary organic aerosol (POA) particles and secondary organic aerosol (SOA) particles. By definition, the former is particulate organic material that is unchanged relative to the forms in which it was emitted to the atmosphere; the latter is particulate organic material that is typically produced from gas phase reactions of primary-emission volatile organic compounds (VOCs) with oxidants such as hydroxyl radical (OH), ozone (O_3), and nitrate radical (NO_3). SOA is thereby composed of secondary compounds with vapor pressures that are low enough to permit significant condensation under ambient conditions.

In addition to POA and SOA as traditionally defined, atmospheric organic particulate matter (OPM) can also contain higher molecular weight (MW) organic compounds that were emitted into the atmosphere as gases, but condensed without having undergone any chemical transformation (*e.g.* oxidation) reactions. Some might argue that such contributions to the OPM be included as POA. Also, there is growing evidence that some gaseous organic compounds can be absorbed by cloud droplets and processed therein to form low vapor pressure products that can contribute to OPM as a type of SOA when the droplets evaporate (Kanakidou *et al.*, 2005).

1.2. POA Sources

Processes that lead to the release of primary organic aerosol materials include burning of fossil fuels (*e.g.* coal, oil), cooking, heating, and biomass burning as in forest fires. There are other sources of POA such as viruses, fungi and bacteria; however these sources are negligible at a global scale. The worldwide emissions of POA materials are estimated to be 9.1, 34.6 and 3.2 Tg y^{-1} for the burning of biofuels (*e.g.* wood), biomass (vegetation), and fossil fuels, respectively. It is believed that POA emissions underwent a dramatic increase in the late of 1800s, decreased in the first half of the nineteenth century, then increased rapidly over the last 60 years due to economic development in China and India (Kanakidou *et al.*, 2005). Table 1.1. shows the regional breakdown of the anthropogenic POA emission estimated by Bond (2004).

Table 1. 1. Regional breakdown of the anthropogenic POA (Tg y^{-1}) adapted from Bond (2004).

Region	POA
open ocean	0.1
Canada	1.0
USA	1.9
Latin America	10.5
Africa	16.8
Oecd Europe	1.3
E. Europe	0.4
CIS (former)	2.0
Middle East	0.5
India region	3.7
China region	4.7
East Asia	2.2
Oceania	1.6
Japan	0.1
World	46.9

1.3. SOA Precursors

1.3.1. Biogenic SOA Precursors

Biogenic volatile organic compounds (VOCs) include isoprene which accounts for approximately half of all biogenic volatile organic compound (BVOC) emissions (Wiedinmeyer *et al*., 2004). Studies have suggested that aqueous phase oxidation of isoprene is a major natural source of SOA formation (Claeys *et al*., 2004b). More than 5000 terpenes such as monoterpenes (C_{10}), diterpenes (C_{20}), and other higher molecular weight compounds have been identified. Excluding isoprene, monoterpenes ($C_{10}H_{16}$) such as α-pinene and β-pinene account for 40-80% of total terpene emissions (Table 1.2.).

Table 1.2. Mass percentage of monoterpene emission as given by Seinfeld and Pankow (2003), Owen *et al*., (2001) and Geron *et al*., (2000). Table adapted from Kanakidou *et al*., (2005*).*

Species	**Mass % Contribution**		
	global	S.Europe and Mediterranean	N. America
α-pinene	24.8	30-58	12-53
β-pinene	16.4	8-33	10-31
Δ3-carene	3.0	0	4-9
limonene	16.4	0-5	6-10
α-ɣ terpinene	0.6	2-5	0-6
terpinolene	1.4	n.d.[a]	0-2
myrcene	3.5	0-4	2-7
ocimene	1.5	0-1	0-1

[a] n.d.: not determined

1.3.2. Emission of Anthropogenic Precursors of SOA

Major emission sources of anthropogenic organic compounds include automobiles and industrial processes. Most of the precursors for anthropogenic SOA are believed to be from emission of aromatic compounds such as benzene, toluene, xylene, and other low molecular weight aromatic compounds (Guenther *et al*., 2000).

Considering that global emission of terpenes has been estimated at 127.4 Tg y^{-1} (excluding isoperene) and assuming that only 15% of that leads to formation of SOA, then an estimated 19.1 Tg of SOA is produced globally by terpenes annually. Comparing this value to the global emission of POA (9 Tg y^{-1}) indicates that the chemical formation of secondary organic aerosols is significant and more research is needed to understand the complex processes involved in the formation of SOA (Kanakidou *et al*., 2005).

1.3.3. SOA Formation Processes

Inasmuch as biogenic monoterpenes appear to be the most significant precursors of SOA formation, more investigation should be conducted with the goal of understanding the reaction processes. Many studies have focused on understanding the kinetics of gas-phase oxidation reactions of monotrepenes with OH, NO_3 and ozone. Studies have shown that of the monoterpene compounds, α-pinene and β-pinene may make the most significant contributions to global SOA formation (Geron *et al*., 2000). Therefore, more research is needed to characterize the oxidation products of these two compounds.

The oxidation of α-pinene with OH, NO_3 and ozone leads to variety of products such as aldehydes, oxy-aldehydes, carboxylic acids, oxy-carboxylic acids, and other compounds. Experiments have suggested that of these three oxidants, ozone has the most significant impact in the formation of SOA (Hoffmann *et al.*, 1997). The oxygenated products need to be relatively nonvolatile in order to remain in the PM phase. Investigations show that product compounds containing sufficient numbers of polar functional groups such as ketones (C=O), aldehydes (H-C=O), alcohols (OH) and carboxylic acids (C(=O)-OH), can have an adequately high tendency to remain in the PM-phase (Yu *et al.*, 1998). According to Bonn and Moortgat (2002), for α-pinene and β-pinene, oxidation with ozone (ozonolysis) has a more significant role in the formation of new particles as compared to oxidation with NO_3 and OH.

1.4. SOA Gas-Particle Partitioning

The oxidation products of semi-volatile organic compounds (SVOC) can partition between the particulate phase and the gas phase. Pankow (1994) developed a simplified application of gas-particle partitioning theory of PM formation.

$$K_{\mathrm{p},i} = \frac{F_i / M_{\mathrm{o}}}{A_i} = \frac{\mathrm{R}T\, f}{10^6\, \overline{\mathrm{MW}}\, \zeta_i p^{\mathrm{o}}_{\mathrm{L},i}} \qquad (1)$$

where, $K_{\mathrm{p},i}$ (m^3 μg^{-1}) is the equilibrium partitioning constant; F_i (μg m^{-3}) is the atmospheric concentration associated with the PM-phase; M_{o} (μg m^{-3}) is mass concentration of SOA produced; A_i (μg m^{-3}) is the concentration in the gas phase; R is the gas constant (m^3 atm mol^{-1} K^{-1}), T (K) is the temperature; f is the weight fraction of

PM phase that is absorbing (considered to unity in this work); $\overline{MW}$ (g mol^{-1}) is the mean molecular weight of the absorbing phase; ζ_i is the mole-fraction based activity coefficient in the absorbing phase; $p^{o}_{L,i}$ (atm) is the vapor pressure (Pankow 1994). Condensation of a component in a multicomponent system is easier than in a single component system because the impurity of the multicomponent system reduces the particle phase activity of the condensing compound.

1.5. Water Interactions

The effect of varying relative humidity (RH) on aerosol particles composed of inorganic materials is well documented; however the effect of varying RH on atmospheric organic particulate matter (OPM) is less certain. Pankow (2010) demonstrated that variations in RH result in two mechanisms that affect condensation of atmospheric OPM.

Mechanism I pertains to OPM that are moderately hygroscopic. Under this mechanism, increasing RH leads to significant uptake of water into the particles, thereby having a considerable affect on atmospheric aerosol mass. The increasing aerosol mass can then draw significantly more organic mass into the particle phase. The result of Mechanism I is a simultaneous significant increase in the aerosol water concentration (M_w) and the aerosol organic concentration (M_o).

Mechanism II acts under conditions where M_o is considerably less than 100% of the total mass of condensable compounds and the system is capable of a significant percentage increase in condensation. Under these conditions, increasing RH can result in significant

increases in M_o, even when condensing OPM is minimally hygroscopic. In contrast, the effect of increasing RH on M_o can be largely insignificant under conditions where condensable organic compounds are nearly 100% condensed.

This study illustrates the importance of considering mechanisms controlling the fraction of atmospheric aerosol mass present as OPM when designing experiments to assess the effects of RH on M_o. "Just as the partitioning of organic compounds to organic aerosols is affected by the amount of water present, so too will the partitioning of water to such aerosols be affected by the amounts and properties of the organic compounds in the aerosols (Seinfeld *et al*., 2001)". Studies show that organic compounds that contain multiple oxygen groups such as alcohols, carboxylic acids, aldehydes and ketones affected more by water in the atmosphere (Seinfeld *et al*., 2001).

Since detailed information on the structure and nature of organic compounds in atmospheric OPM is always missing, it is difficult to estimate the thermodynamic properties of the compounds (vapor pressure, enthalpy of vaporization, etc.) Consequently; most of the models used to predict SOA formation are limited in that they neglect the role of water (Kanakidou *et al*., 2005). In this work structures of organic compounds that are involved in the formation of SOA will be estimated without neglecting the role of water in the process.

1.6. Governing Equations

Eq. (2) came from Eq.(1), since the SOA phase also contains water, the total SOA concentration M_t ($\mu g\ m^{-3}$) is calculated by Eq.(3) (Pankow *et al*., 2001):

$\frac{F_i}{A_i} = M_{\mathrm{o}}\, K_{\mathrm{p},i}$ (2)

$M_{\mathrm{t}} = M_{\mathrm{w}} + M_{\mathrm{o}}$ (3)

The fractional mass yield (Y_{o}) of formation of SOA by oxidation reaction of parent hydrocarbon is defined as (Pankow *et al*., 2001):

$Y_{\mathrm{o}} = \frac{M_{\mathrm{o}}}{\Delta \mathrm{HC}}$ (4)

$Y_{\mathrm{w}} = \frac{M_{\mathrm{w}}}{\Delta \mathrm{HC}}$ (5)

$Y_{\mathrm{t}} = \frac{M_{\mathrm{t}}}{\Delta \mathrm{HC}} = Y_{\mathrm{o}} + Y_{\mathrm{w}}$ (6)

Where ΔHC (μg m^{-3}) is the amount of parent hydrocarbon that involves in the reaction.

$Y = \sum_i^n \alpha_i$ (7)

Using Odum *et al*., formula for calculating the overall yield:

$Y = \sum_i \alpha_i \left(\frac{K_{\mathrm{p,om},i}\, M_{\mathrm{o}}}{1 + K_{\mathrm{p,om},i}\, M_{\mathrm{o}}} \right)$ (8)

Where $\alpha_i$is the stoichiometric coefficient giving the mass fraction of ΔHC that leads to the hypothetical single condensable product:

$T_i = A_i + F_i = 10^3\, \alpha_i\, \Delta \mathrm{HC}$ (9)

2. Methods

2.1. Volatility Basis Set (VBS)

The VBS (volatility basis set) as proposed by Donahue *et al*., (2006) has become a popular means for binning the range of products formed by the oxidation of a parent hydrocarbon that can lead to the formation of secondary organic aerosol (SOA) particulate material. The classification of compounds into different volatility bins is based on the values of the saturation concentration C^* (=1/K_p, µg m^{-3} where, K_p is the equilibrium partitioning constant). Compounds with the highest C^* values are the most volatile and the compounds with the lowest C^* values are the least volatile. Typically, the VBS approach is used with C^* values ranging from 0.01 µg m^{-3} to 10^6 µg m^{-3}. For the purpose of this investigation, C^* values of 10^5 µg m^{-3} and 10^6 µg m^{-3} have been neglected because compounds with such high volatilities do not reside in the PM phase to any significant extent. Table 2.1. gives the C^* values and mass yields that were derived by Donahue *et al*., (2009) as fitted parameters from chamber experiments (α_i) by the reaction of α-pinene with ozone.

Table2. 1. Fitted VBS Parameters of Donahue *et al*., (2009) Based on α-Pinene/Ozone Chamber Experiments.

	Bin						
Property	1	2	3	4	5	6	7
α_i	0.400	0.183	0.120	0.086	0.051	0.000	0.004
C_i^* (µg m^{-3})	10000	1000	100	10	1	0.1	0.01
$K_{p,i}$ (m^3 μg^{-1})	0.0001	0.001	0.01	0.1	1	10	100

To identify possible structures of the compounds constituting each bin, *i.e.*, for the K_p value of each bin, two steps were used. Step1 is based on the absorptive partitioning equation of Pankow (1994) Eq. (1).

In the application of Step 1, the molecular weight of each compound is estimated based on the assumption that the compound consists of 10 carbons and some mix of four major functional groups, namely –OH (alcohol), –CHO (aldehyde), –CO– (ketone), and –COOH (carboxylic acid). At the conclusion of Step 1, log p^{o}_{L} was estimated for the bin assuming T = 298 K.

Step 2 involved the use of the group contribution method SIMPOL.1 to predict the vapor pressure of the compound at T = 298 K based on the functional groups present. This method utilized Eq.(10) (Pankow and Asher 2008):

$$\log p^{o}_{L,i}(T) = \sum_{k} \nu_{k,i}\, b_k(T) \quad k = 0, 1, 2, 3 \ldots \quad (10)$$

Where $\nu_{k,i}$ is the number of groups of type k in i; $b_k(T)$ is the group contribution term for group k and b_0 (T) is pertaining to group zero with $\nu_{0,i} \equiv 1$ for all i. For each set of k values tested, Eq.(10) was used with the values in Table 2.2 . to calculate log p^{o}_{L}, which was compared with the value from STEP 1. Step 2 was repeated in a search for all possible combinations of functional groups such that the value of log p^{o}_{L} from Step 2 was within ±0.5 of log p^{o}_{L} obtained using Step 1. Table 2.3. provides a summary of the results for each bin.

Table 2.2. Chemical groups used in SIMPOL.1 and the $B_{k,i}$ values from Pankow and Asher 2008.

group	*k*	coefficient	footnote comment	$B_{k,1}$	$B_{k,2}$	$B_{k,3}$	$B_{k,4}$
zeroeth group	0	b_0	a	-4.26938E^{+2}	2.89223E^{-1}	4.42057E^{-3}	2.92846E^{-1}
carbon number	1	b_1	b	-4.11248E^{+2}	8.96919E^{-1}	-2.48607E^{-3}	1.40312E^{-1}
hydroxyl	7	b_7	c	-7.25373E^{+2}	8.26326E^{-1}	2.50957E^{-3}	-2.32304E^{-1}
aldehyde	8	b_8	d	-7.29501E^{+2}	9.86017E^{-1}	-2.92644E^{-3}	1.78077E^{-1}
ketone	9	b_9	e	-1.37456E^{+1}	5.23486E^{-1}	5.50928E^{-4}	-2.76950E^{-1}
carboxylic acid	10	b_{10}	f	-7.98796E^{+2}	-1.09436E^{+0}	5.24132E^{-3}	-2.28040E^{-1}

[a] use for all compounds *i* with $_{0,i} = 1$

[b] use for all compounds *i* with $_{1,i}$ = total number of carbons in the molecule

[c] use with the total number of hydroxyl groups attached to non-aromatic carbons

[d] use with the total number of aldehyde groups

[e] use with the total number of ketone groups

[f] use with the total number of carboxylic acid groups

Table 2.3. Possible structures and estimated vapor pressure for each bin at 298 K.

a: carbon number, *b*: ketone number, *c*: aldehyde number, *d*: alcohol number, *e*: carboxylic acid number, *x*: CH number, *y*:CH_2 number and *z*: CH_3 number.

Bin number	Compound name	MW (g mol^{-1})	O/C atomic ratio	Fitted log p^o_L	SIMPOL.1 log p^o_L	Ave log p^o_L
Bin 1	*a_bcde_xyz*					
	10_2100_221	182	0.3	-5.596	-5.90	-5.87
	10_0110_333	172	0.2	-5.907		
	10_1200_222	184	0.3	-5.979		
	10_0300_232	185	0.3	-6.362		
Bin 2						
	10_2010_222	185	0.3	-6.460	-6.90	-6.88
	10_3100_111	197	0.4	-6.532		
	10_0020_343	174	0.2	-6.770		
	10_1110_232	186	0.3	-6.843		
	10_1300_221	198	0.4	-7.299		
Bin 3						
	10_1020_332	187	0.3	-7.707	-7.90	-7.90
	10_2110_221	199	0.4	-7.780		
	10_2001_221	198	0.4	-7.789		
	10_0120_333	189	0.3	-8.090		
	10_1101_222	200	0.4	-8.172		
	10_1210_222	201	0.4	-8.163		
Bin 4						
	10_0310_232	202	0.4	-8.546	-8.90	-8.92
	10_0201_232	201	0.4	-8.555		
	10_3001_111	213	0.5	-8.725		
	10_0030_343	191	0.3	-8.954		
	10_1120_232	203	0.4	-9.027		
	10_1011_232	202	0.4	-9.036		
	10_2101_121	214	0.5	-9.108		
Bin 5						
	10_0002_332	201	0.4	-9.428	-9.90	-9.93
	10_1201_221	214	0.5	-9.491		
	10_0301_222	216	0.5	-9.875		
	10_1030_332	204	0.4	-9.890		
	10_2011_221	215	0.5	-9.972		
	10_0130_333	206	0.4	-10.273		
	10_0021_333	205	0.4	-10.283		
Bin 6						
	10_0211_232	218	0.5	-10.738	-10.90	-11.03
	10_0102_232	217	0.5	-10.747		
	10_1021_232	219	0.5	-11.219		
Bin 7						
	10_0121_332	219	0.5	-11.602	-12.00	-11.96
	10_0012_332	218	0.5	-11.611		
	10_1102_221	230	0.6	-11.684		

2.2. The Combinatorial Aerosol Formation Method

The Combinatorial Aerosol Formation Model (CAFM) is a deterministic model that was used to determine the amount of organic mass (M_o µg m^{-3}) that would form at T = 298 K assuming certain ΔHC and RH values, the α_i values in Table 1, and each of the possible combinations of the structures in Table 2.3. The model considers every possible combination of the structures in the bins. CAFM works with a maximum of 50 bins and an unlimited number of structures in each bin. In this work, seven bins were considered. The numbers of structures in Bins 1 through 7 are 4, 5, 6, 7, 7, 3 and 3. Since $\alpha_6 = 0$, the variability in bin 6 had no effect, and the number of possible combinations that needed to be considered for each value of ΔHC and RH was 4×5×6×7×7×3 = 17640. In computing M_o, values of the activity coefficient (ζ_i) were obtained using UNIFAC. Water uptake in the reaction was investigated as RH varied from 0 to 90% in increments of 10%; the range of ΔHC considered was 5µg m^{-3} to 200 µg m^{-3}.

2.3. Mathematical Modeling

Eq.(20) of Pankow (1994) gives the relationship between the vector of F_i values and the vector of T_i as defined by the matrix equation, where each partitioning compound satisfies its own version of Eq. (1).

$$\begin{bmatrix} F_1 \\ . \\ F_n \end{bmatrix} = \frac{RT\ f\ M_t}{10^6\ \overline{\mathrm{MW}}} \begin{bmatrix} \frac{\left(\zeta_1 p^{\mathrm{o}}_{\mathrm{L},1}\right)^{-1}}{1+K_{\mathrm{p,om,1}}\ M_{\mathrm{o}} f} & . & . \\ . & . & . \\ . & . & \frac{\left(\zeta_{\mathrm{n}} p^{\mathrm{o}}_{\mathrm{L},n}\right)^{-1}}{1+K_{\mathrm{p,om,n}}\ M_{\mathrm{o}} f} \end{bmatrix} \begin{bmatrix} T_1 \\ . \\ T_{\mathrm{n}} \end{bmatrix} \quad (11)$$

For a given guess value $M_{t,guess}$ and measured vector *T*, Pankow (1994) discusses how Eq. (11) can be solved iteratively to yield a corresponding vector *F*. Iteration is required because for each step the vector *F* does not necessarily satisfy the relationship:

$$\sum_i F_i = 1000\, M_{\mathrm{t,guess}} \quad (12)$$

Finding the desired vector of SOA concentrations *F* can be achieved iteratively by choosing successive $M_{\mathrm{t,guess}}$ values, obtaining successive *F* solutions, and thereby minimizing the variable ϵ to within some small tolerance of zero.

$$\epsilon = [\, \sum_1^n F_i - 1000\, M_{\mathrm{t,guess}} \,] \quad (13)$$

For each iteration CAFM gives: the amount of organic PM in each bin M_i (μg m^{-3}) and the total of those values M_o (μg m^{-3}); the mean molecular weight of the PM-phase $\overline{MW}$ (g mol^{-1}); the concentration of water M_w (μg m^{-3}) in the PM; M_t (μg m^{-3}) (the sum of M_w and M_o); mass fraction of each structure X_i; concentration of each structure C_i (ppm). Eq. (14) represents the relationship between M_i, M_o, (Pankow 1994)

$$M_o = \sum_i M_i\, X_i \quad (14)$$

Using Microsoft Excel spreadsheet, the relationship between the amounts of organic mass formed and the amount of water uptake at various RH and ΔHC was determined. To investigate the relative contribution of each bin to the trending behavior that was observed, the mass of the organic mass formed in each bin was also plotted as function of water uptake at various RH and ΔHC. The spreadsheet was useful in identifying the general trends, however; it was limited in that the exact combination of structures

responsible for the observed trends could not be identified. To compensate for this limitation, Grapher 9 software was used. Grapher 9 software gives the benefit of isolating different regions of the M_i VS. M_w plots and identifying different structures in it. Figure 2.1. shows a snapshot of the output from the Grapher 9 software.

Fig 2.1. The distribution of the structures of Bin 7 versus water uptake, ΔHC= 50 μg m^{-3}, RH=80%. T=298 K.

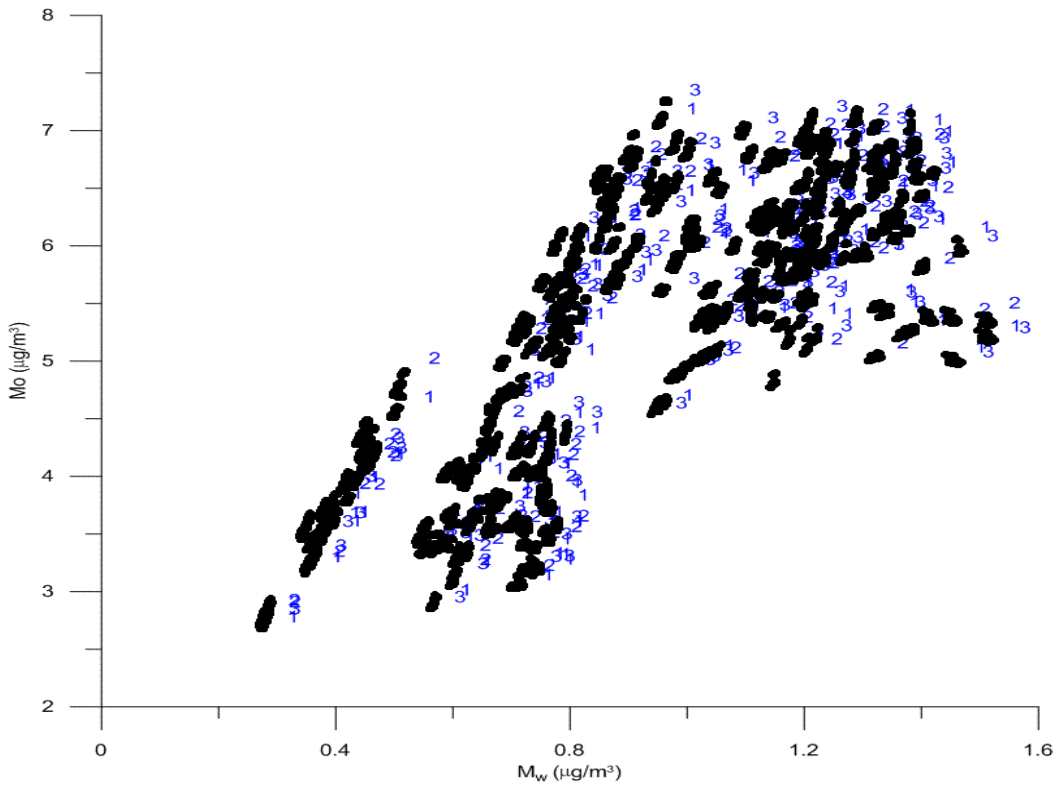

3. Results and Discussion

The goal of this work as was to determine how a variety of structural combinations affects M_o and M_w over a range of RH values and a range of ΔHC values. From Table 3.1, it can be observed that ΔHC of 5 μg m^{-3} produced a negligible arithmetic mean level of M_o at all RH values considered, and so that value of ΔHC is not very useful for this investigation. Therefore, this work emphasizes the distributions of M_o values formed at higher ΔHC values, in particular 10, 30, and 50 μg m^{-3}.

Table3. 1. Model Predictions for Arithmetic Mean Values of M_o, M_w and M_t (μg m^{-3}).

	Relative Humidity (RH)											
	0%			30%			50%			90%		
ΔHC	M_o	M_w	M_t	M_o	M_w	M_t	M_o	M_w	M_t	M_o	M_w	M_t
5	0.00971	0	0.00971	0.0249	0.000770	0.0257	0.0383	0.00241	0.0407	0.0938	0.0202	0.114
10	0.0992	0	0.0992	0.150	0.00477	0.155	0.200	0.0126	0.213	0.372	0.0799	0.452
30	1.131	0	1.131	1.460	0.0447	1.505	1.744	0.105	1.849	2.489	0.494	2.983
50	3.031	0	3.031	3.690	0.109	3.799	4.197	0.244	4.441	5.470	1.041	6.511
100	9.893	0	9.893	11.270	0.320	11.590	12.320	0.685	13.005	14.990	2.709	17.699
200	28.590	0	28.590	31.380	0.854	32.234	33.510	1.790	35.300	38.810	6.713	45.523

As part of the interpretation of the results, statistical analyses were performed for RH = 80% while varying ΔHC from 10 to 100; Figures 3.1 and 3.2 show the frequency distribution plots for M_o and M_w produced from the different structural combinations. From the plots, it can be seen that the data are not normally distributed. At ΔHC = 10 μg m^{-3}, the M_o and M_w are quite scattered. As the ΔHC increases above 10 μg m^{-3}, the distributions become more regular. Because of bimodal behavior of M_o and M_w, more investigation was carried out on the effects of the structures on the extent of organic mass formation.

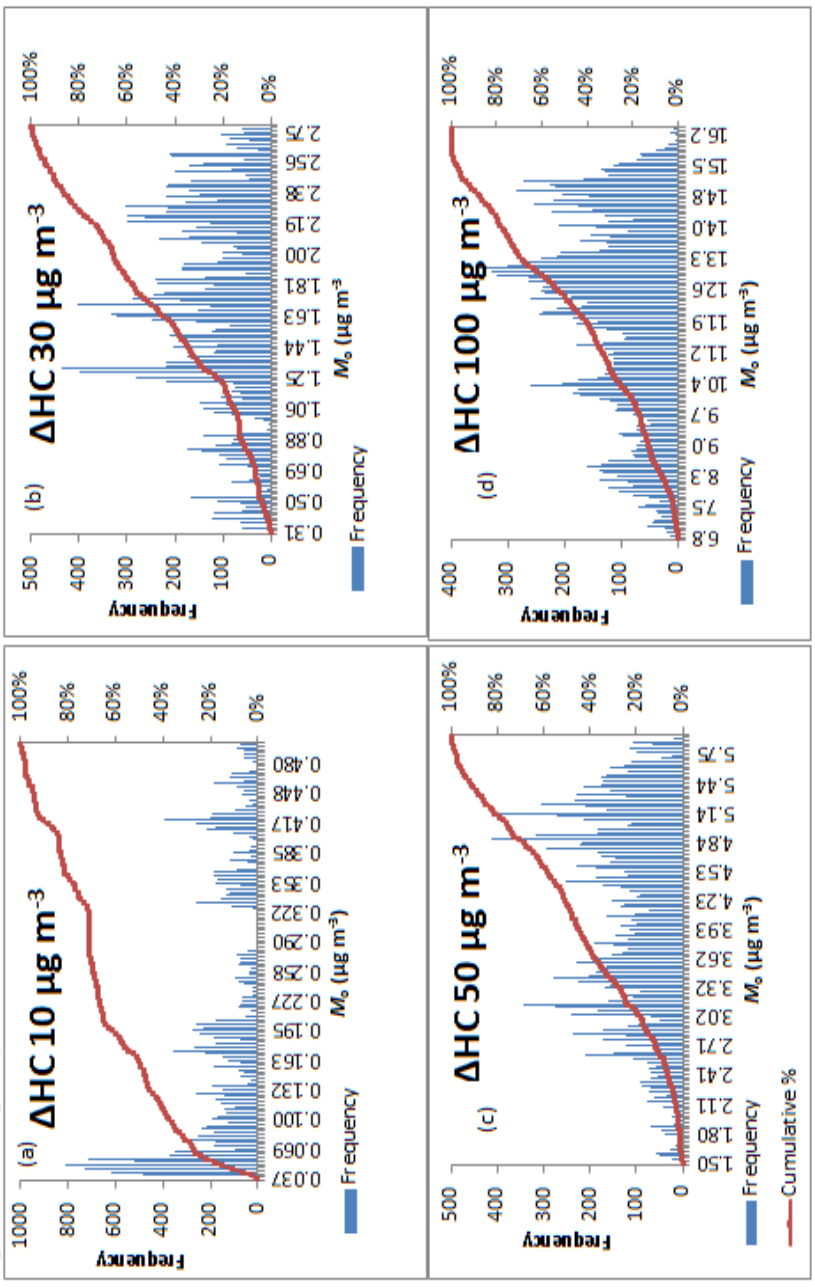

Figure 3.1. Frequency distributions for M_0 at various levels of ΔHC when RH = 80%., T = 298 K.

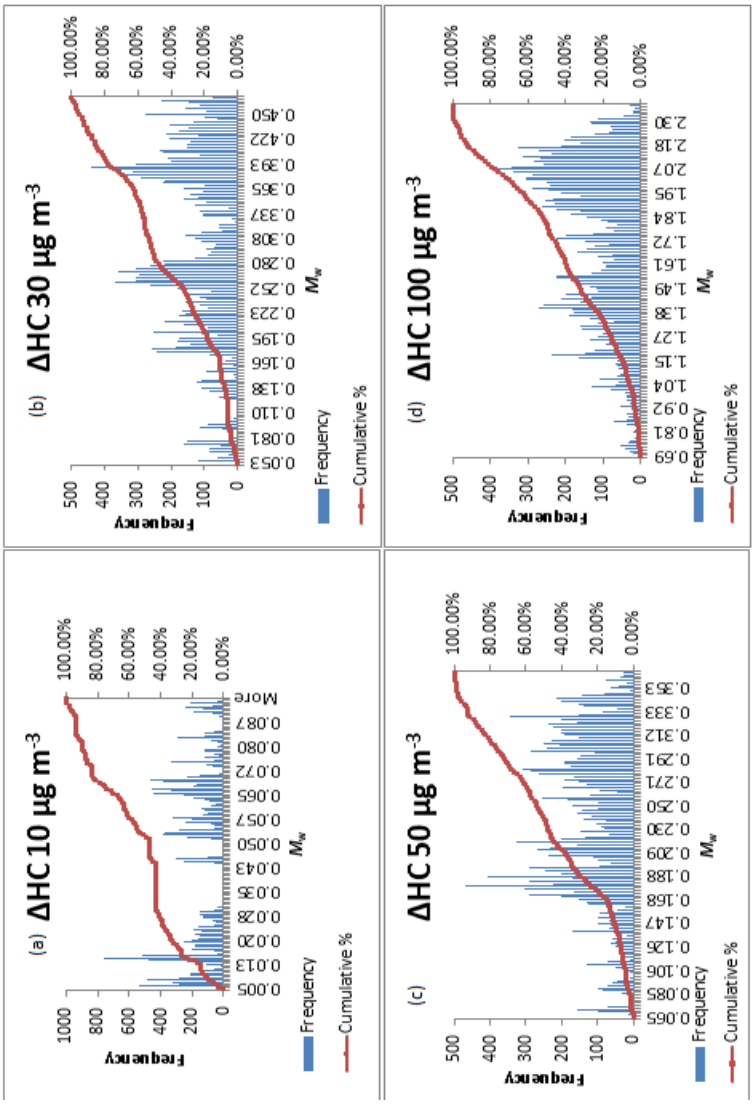

Figure 3.2. Frequency distributions for M_w at various levels of ΔHC when RH = 80%., T = 298 K.

Scatter plots of M_o vs. M_w at different values of ΔHC and RH are shown in Figures 3.3a, 3.4a, 3.5a, and 3.6a. The other panels show the condensed mass concentrations for the individual bins (1, 2, 3, 4, 5 and 7 respectively). For example, Figures3.3.g. and 3.4.g show the distributions of M_7 (bin 7) when RH = 20% and 80%, respectively, when ΔHC = 10 μg m^{-3}. At low RH the variety of structural combinations leads to more variation in M_o than at high RH. Figures 3.5.g. and 3.6.g show the distribution of M_7 for bin 7 under the conditions where RH = 20 and RH = 80 respectively, when ΔHC = 100 μg m^{-3}.

Figure 3.3. M_o and M_i values vs. M_w when ΔHC = 10 μg m^{-3}, RH = 20% and T = 298 K

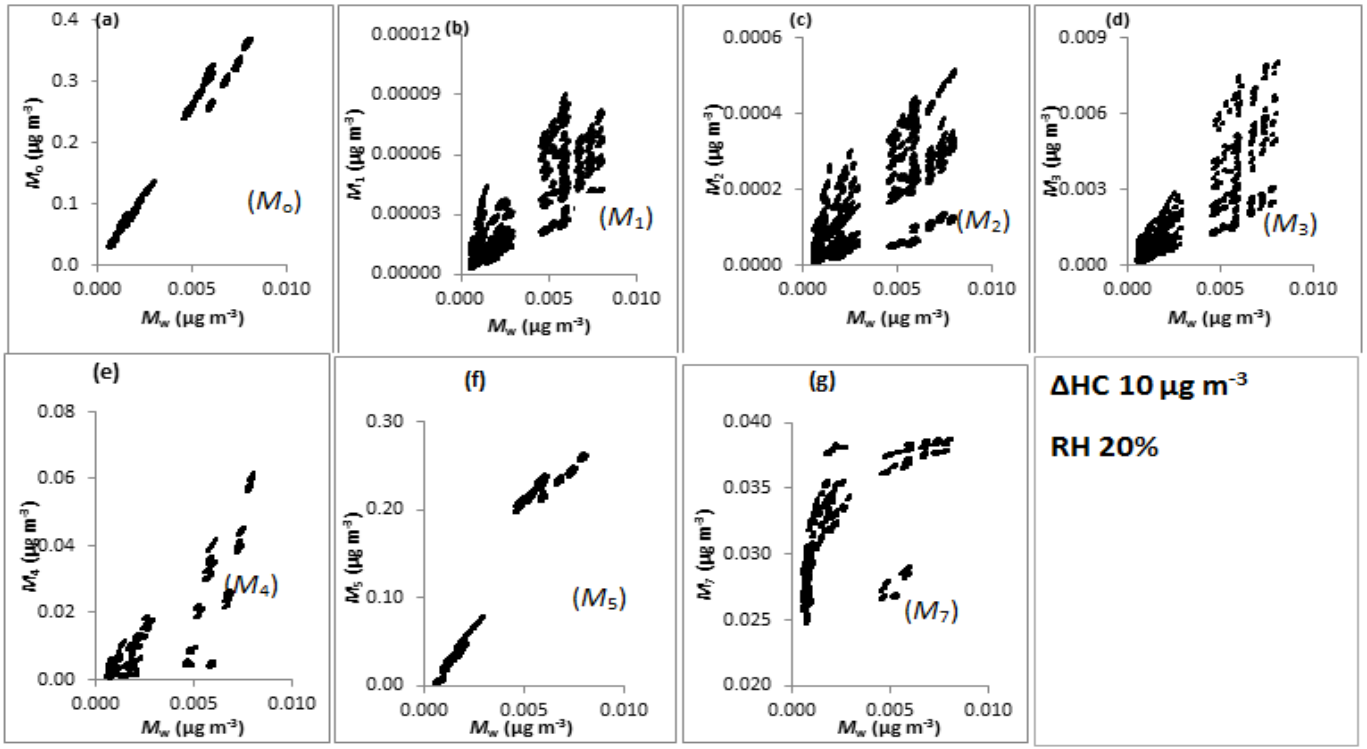

Figure 3.4. M_o and M_i values vs. M_w when ΔHC = 10 μg m^{-3}, RH = 80% and T = 298 K.

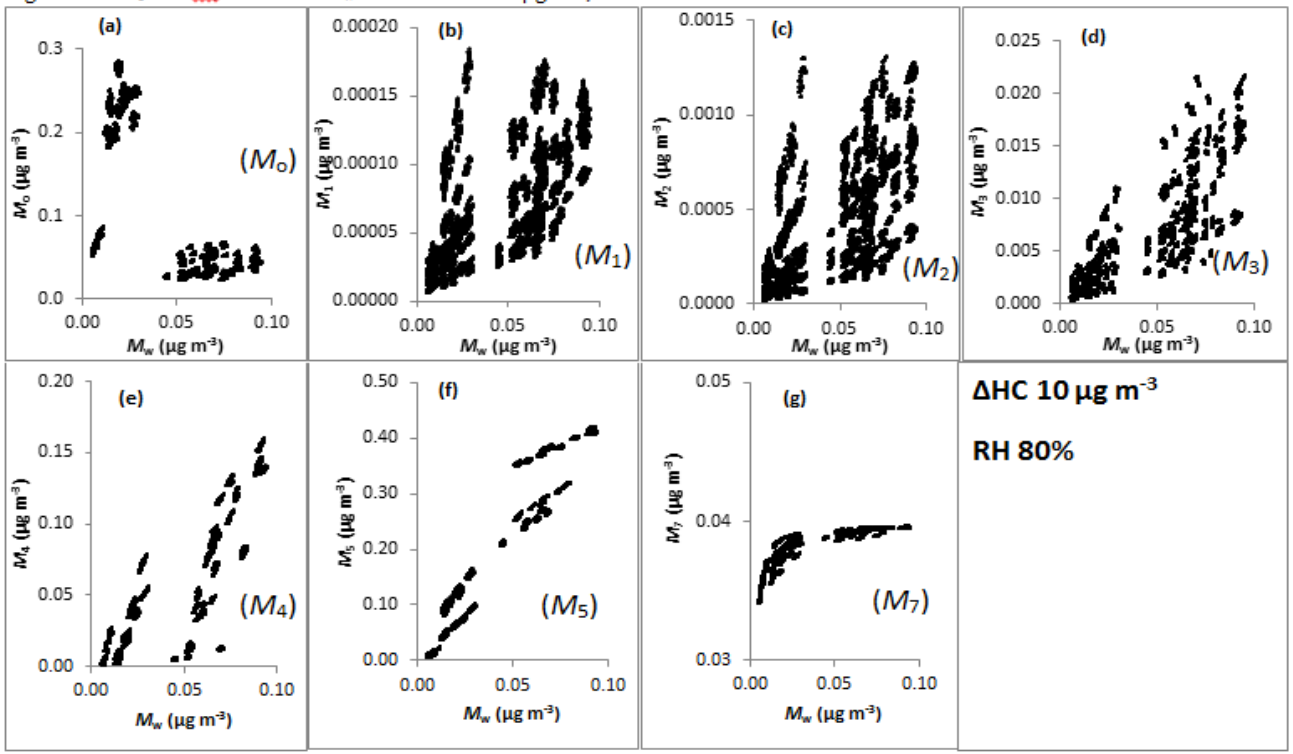

Figure 3.5. M_o and M_i values vs. M_w when ΔHC = 100 µg m^{-3}, RH = 20% and T = 298 K.

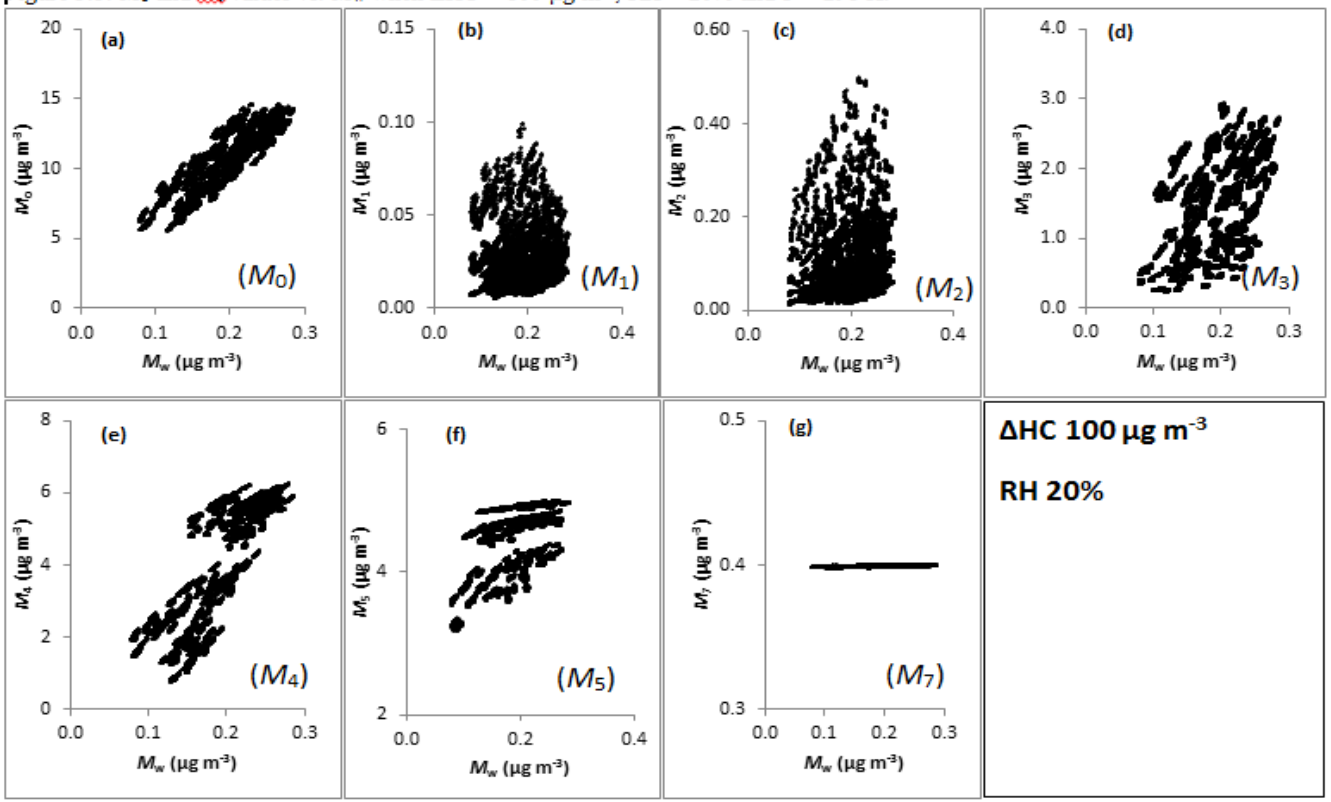

Figure 3.6. M_0 and M_i values vs. M_w when ΔHC = 100 μg m^{-3}, RH = 80% and T = 298 K.

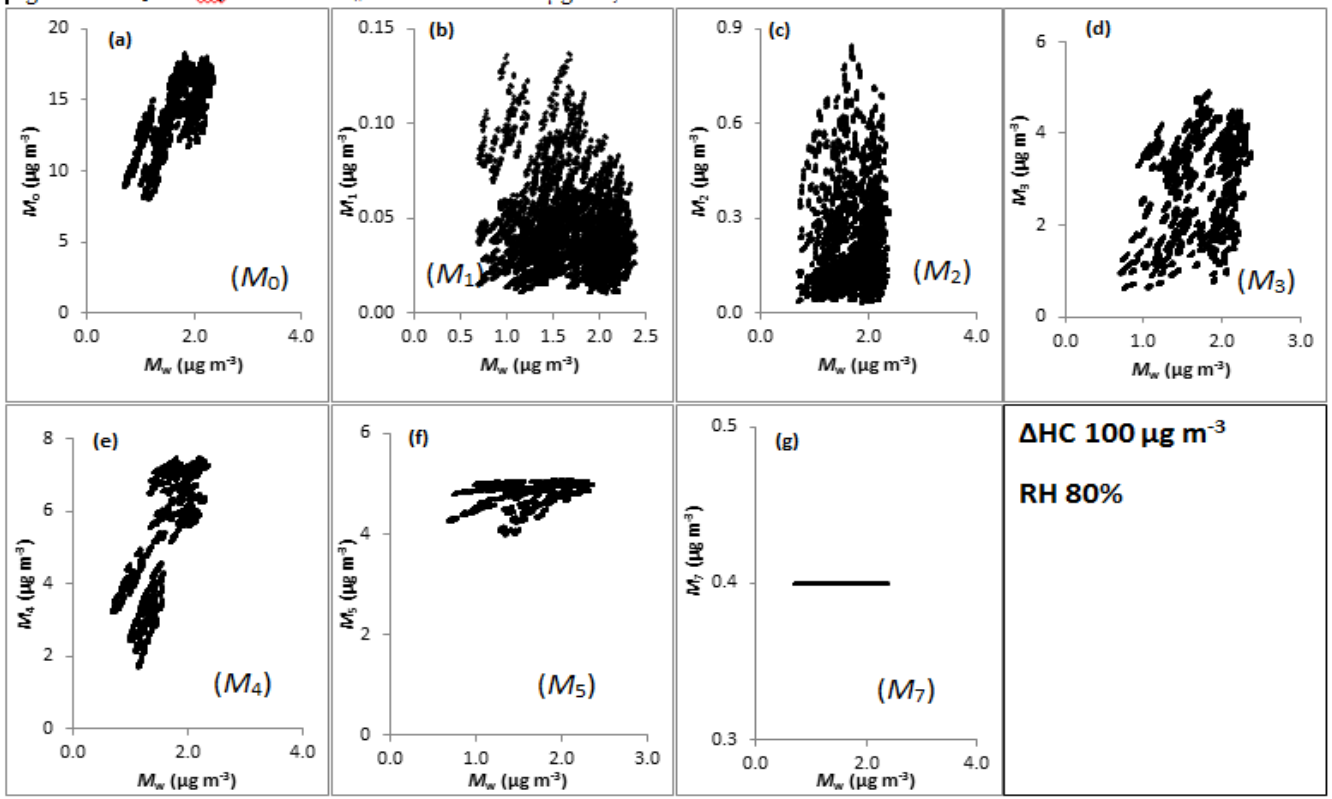

At any given pair of RH and ΔHC values, M_w and M_o will of course depend on the combination of specific structures that is assumed. The results from different combinations are presented in Figure 3.7.a. for RH = 80% and ΔHC = 50 μg m^{-3}, and it is evident that there are some observable trends. However, it is not clear from Figure 3.7.a which bin has the most effect on M_o. Values of the single-bin contributions to M_o versus M_w are presented in Figures 3.7.b, 3.7.c, 3.7.d, 3.7.e, 3.7.f and 3.7.g. As it was mentioned the main functional groups of focus are ketones, aldehydes, alcohols and carboxylic acids. The first two groups are abundant in lower-numbered bins while the last two groups are abundant in the higher-numbered bins. Plots of organic mass as function of water uptake for bins 1, 2, and 3 do not show any trends, while for bins 4 and 5, show some trends and for bin 7 remains constant. The behavior of M_4 and M_5 versus M_w is because the structures with more polar functional group that has higher affinity for water included in these bins, and therefore; more of the compounds partition into the PM phase. Focusing on the results for bin 7 (see Figure 3.7.g), the amount of organic mass formed remains constant. This observation was expected because the structures that constitute bin 7 are highly polar, and therefore; tend to reside in the PM phase, with minimal influence from the structural combinations and water uptake.

Figure 3.7. M_o and M_i values vs. M_w when ΔHC = 50 µg m^{-3}, RH = 80% and T = 298 K.

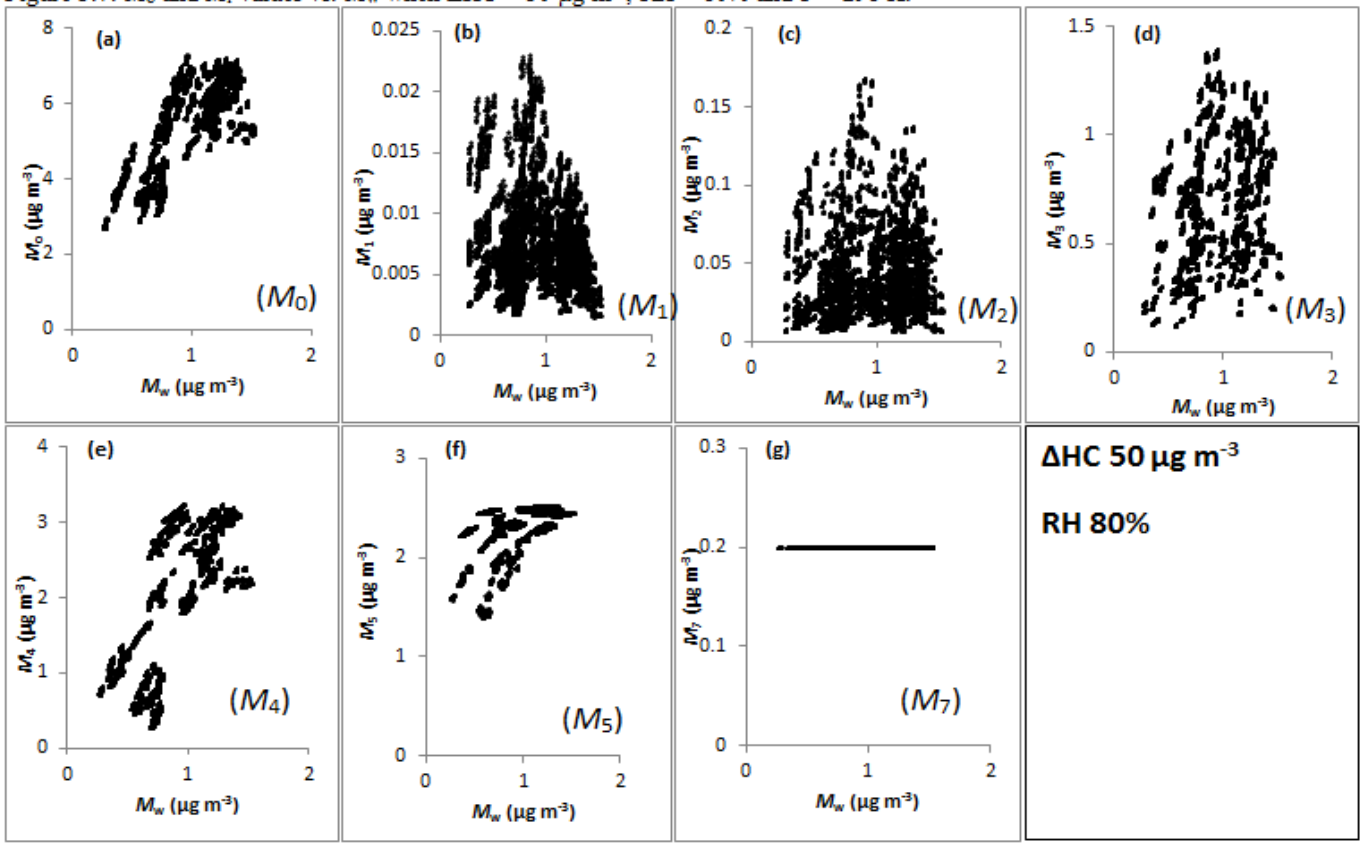

To explain the trends observed for bins 4 and 5 (see Fig. 3.7.e and 3.7.f), the Grapher 9 software package was used. This software has the ability to identify the combination of structures responsible for the trends observed. For example, considering structure 1 from bin 4, which consists of three aldehyde groups and one alcohol group, the amount of water uptake and the amount of organic mass formed is generally low. Generally, it would be expected that the more water uptake the more organic mass would be produced, but is in contrast with the results in figure 3.8. At a water uptake of approximately 0.4, the amount of organic mass is approximately 1, while at water uptake of 0.7, the amount of organic mass formed is approximately 0.6. The reason for this behavior is that the amount of organic mass produced in each bin is influenced by the structures form other bins. Similarly, considering structure 7, which consists of two ketone groups, one aldehyde group and one carboxylic acid group, it can be seen that the amount of water uptake and the amount of organic mass produced is generally higher when this structure participates. The same observation is made in bin 5 (see Fig.3.9).

Figure 3.8. organic mass distribution of bin 4 versus water uptake, at ΔHC = 50 µg m^{-3}, RH = 80% and *T* = 298 K.

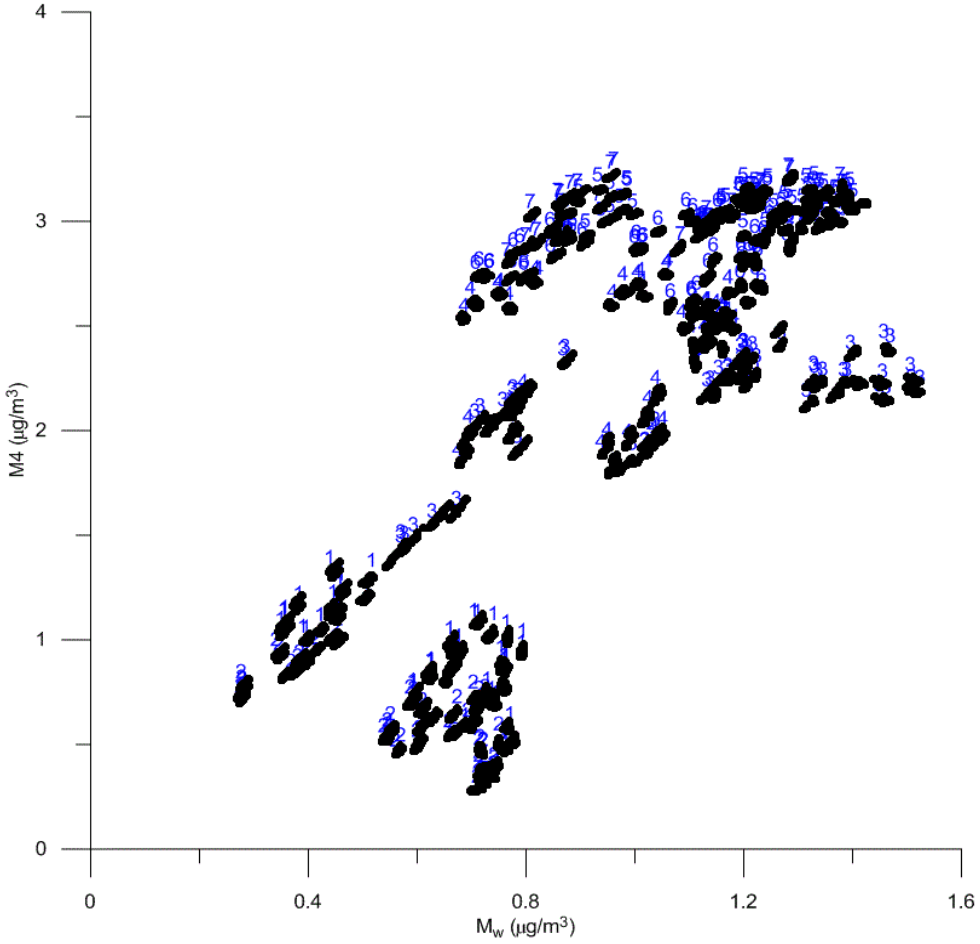

Figure 3.9. organic mass distribution of bin 5 versus water uptake, at ΔHC = 50 µg m^{-3}, RH = 80% and *T* = 298 K.

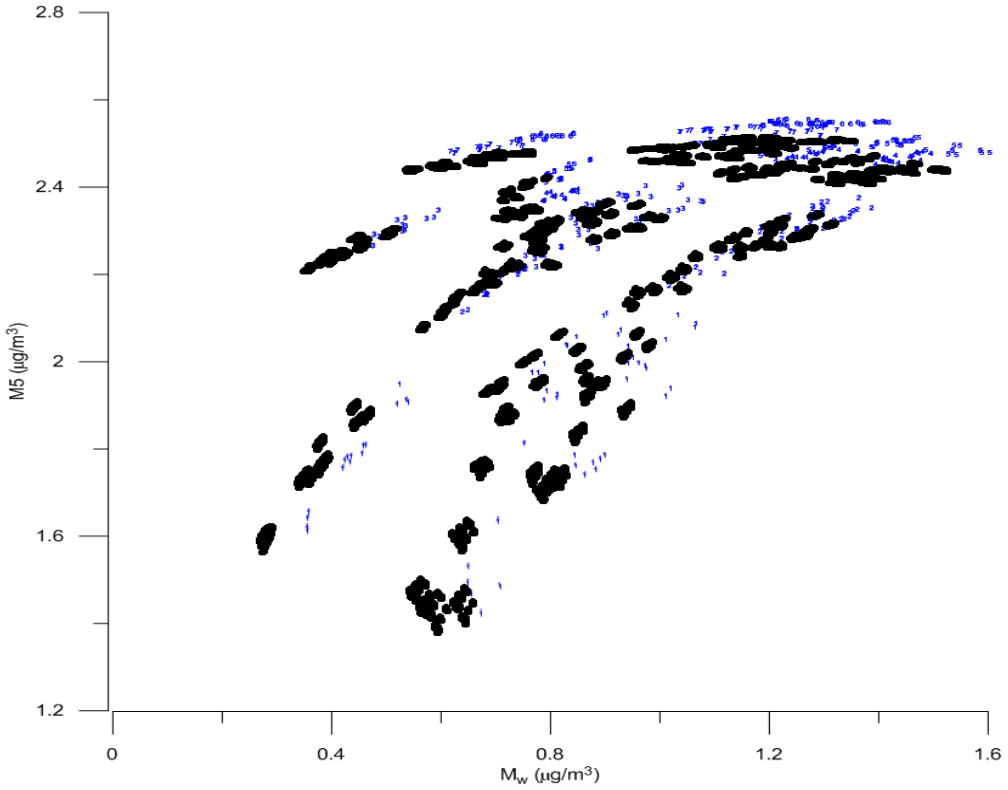

Most of the organic mass was produced in bin 4. For this reason, more investigation was done for bin 4 to explain the observed behavior. Using Grapher 9 and Microsoft Excel, the plot in figure 3.8., was divided into different regions, and the structures that lie in each of those regions were identified. Figure 3.10. shows the relationship between water uptake and the amount of organic mass produced in bin 4 when structure 3 interact with different structural combinations from other bins. For example, considering the M_w between 0.8 and 0.9, M_4 between 1.8 and 2, the structures 5 and 1 from bin 3 and 5 respectively are always involved, while the combination of other structures changes. Almost the same trends can be observed when considering the interaction of structure 7 of bin 4 with other combinations (see figure 3.11).

Figure 3.10. Organic mass distribution of structure 3 in bin 4 versus water uptake, ΔHC = 50 μg m^{-3}, RH = 80% and T = 298 K.

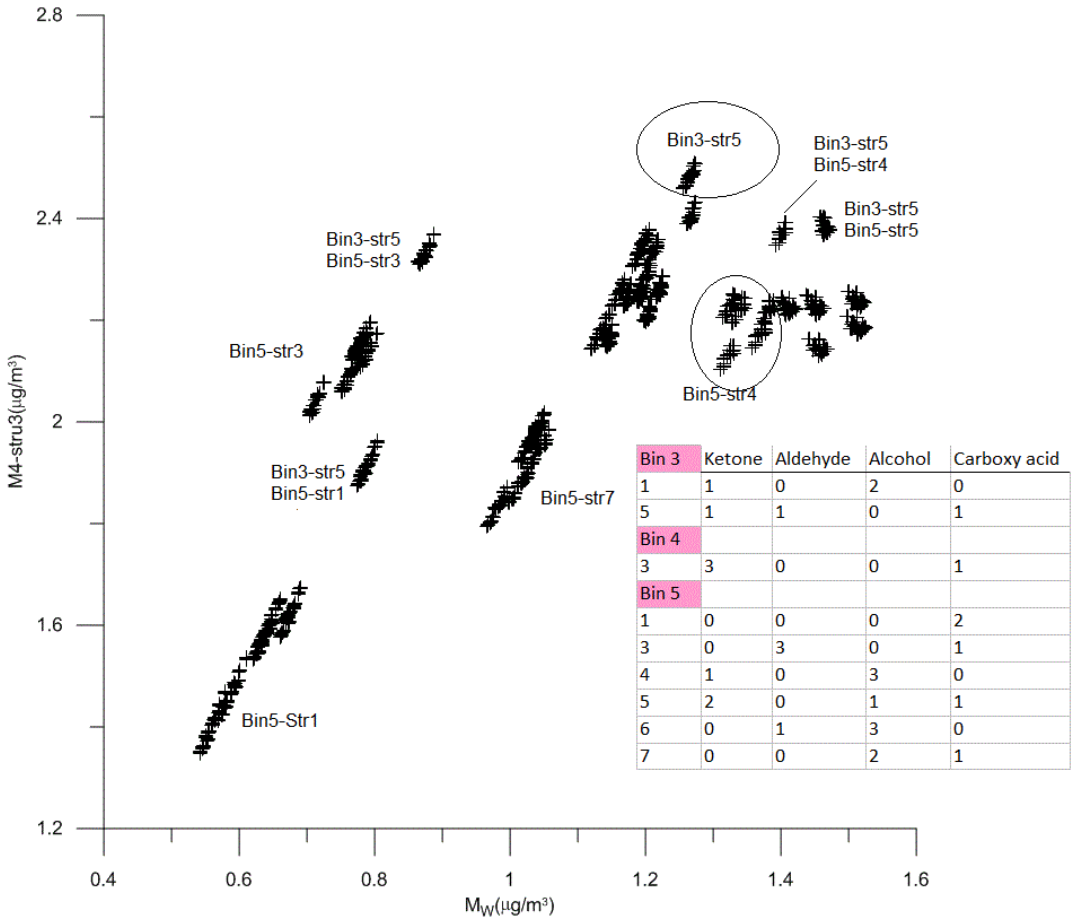

Bin 3	Ketone	Aldehyde	Alcohol	Carboxy acid
1	1	0	2	0
5	1	1	0	1
Bin 4				
3	3	0	0	1
Bin 5				
1	0	0	0	2
3	0	3	0	1
4	1	0	3	0
5	2	0	1	1
6	0	1	3	0
7	0	0	2	1

Figure 3.11. Organic mass distribution of structure 7 in bin 4 versus water uptake, ΔHC = 50, μg m^{-3}, RH = 80% and T = 298 K.

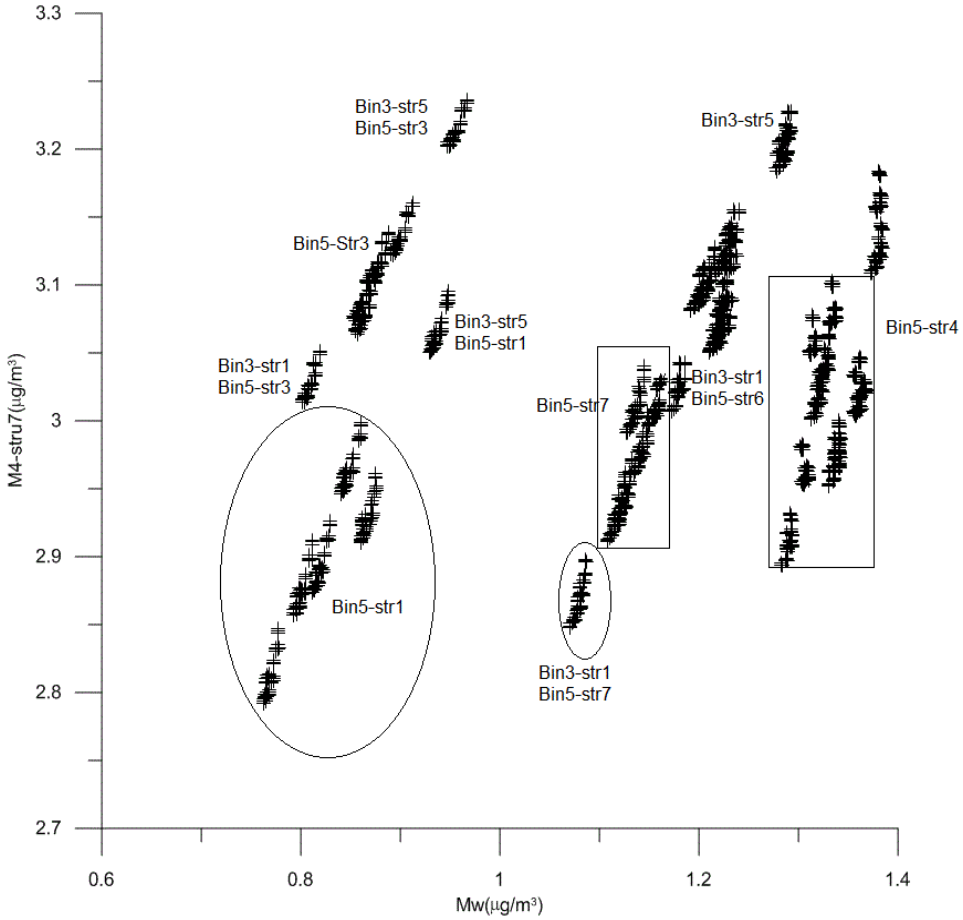

4. Conclusion

SOA plays an important role impacting climate change and human health; therefore it is important to discover models that determine the structure and nature of molecules contributing to SOA formation. These discoveries are opening a window to a new level of studying the whole system. SOA formation investigated in the present work is characterized by the oxidation products of α-pinene and ozone. Results show that the amount of SOA that is formed is almost negligible when the amount of parent hydrocarbon involved in the reaction is low (*i.e.* around 5 μg m^{-3}), especially at lower RH. The predicted structures from bins 1, 2 and 3 mainly comprised of ketone and aldehyde groups did not show any noticeable change and trend in SOA formation due to amount of water uptake. Furthermore, no relationship was found between the amount of M_i formation and influence from other compounds mainly comprised of bins 4, 5 and 7. Observing bins 4 and 5 compounds with a greater number of polar groups (alcohol and carboxylic acid) indicates that structure has a significant effect on organic mass formation. This observation is in agreement with the fact that the more hydrophilic the compound is, the higher RH, leading to more condensation into the PM phase. This study indicates that structure and water uptake have an effect on SOA formation for certain bins. However more investigation is needed in order to determine the contribution of the many other molecular structures on the formation of SOA.

5. References

Bond, T. C., Streets, D. G., Yarber, K. F., Nelson, S. M.,Woo, J. H., and Klimont, Z.: A technology-based global inventory of Black and Organic Carbon emissions from Combustion, J. Geophys. Res., 109, D14203, doi:10.1029/2003JD003697, 2004.

Bonn, B. and Moortgat, G. K.: New particle formation during alpha- and beta-pinene oxidation by O3, OH and NO3, and the influence of water vapor: particle size distribution studies, Atmos. Chem. Phys., 2, 183–196, 2002.

Claeys, M., Wang, W., Ion, A. C., Kourtchev, I., Gelencser, A., and Maenhaut, W.: Formation of secondary organic aerosols from isoprene and its gas-phase oxidation products through reaction with hydrogen peroxide, Atmos. Environ., 38, 4093–4098, 2004b.

Donahue, N. M., Robinson, A. L., Stanier, C. O., and Pandis, S. N.: Coupled partitioning, dilution, and chemical aging of semivolatile organics, Environ. Sci. Technol., 40, 2635–2643, 2006.

Donahue, N.M., Robinson A.L., Pandis S.N.: Atmospheric organic particulate matter: From smoke to secondary organic aerosol. Atmos Environ 43:94–106, 2009.

Geron, C., Rasmussen, R., Arnts, R. R., and Guenther, A.: A review and synthesis of monoterpene speciation from forests in the United States, Atmos. Environ., 34, 1761–1781, 2000.

Guenther, A., Geron, C., Pierce, T., Lamb, B., Harley, P., and Fall, R.: Natural emissions of non-methane volatile organic compounds, carbon monoxide, and oxides of nitrogen from North America, Atmos. Environ., 34, 2205–2230, 2000.

Hoffmann, T., Odum, J. R., Bowman, F., Collins, D., Klockow, D., Flagan, R. C., and Seinfeld, J. H.: Formation of Organic Aerosols from the Oxidation of Biogenic Hydrocarbons, J. Atmos. Chem., 26, 189–222, 1997.

Kanakidou, M., Seinfeld, J. H., Pandis, S. N., Barnes, I., Dentener, F.J., Facchini, M.C., Van Dingenen, R., Ervens, B., Nenes, A., Nielsen, C.J., Swietlicki, E., Putaud, J.P., Balkanski, Y., Fuzzi, S., Horth, J., Moortgat, G. K., Winterhalter, R., Myhre, C.E.L., Tsigaridis, K., Vignati, E., Stephanou, E.G., and Wilson, J.: Organic aerosol and global climate modelling: a review, Atmos. Chem. Phys., 5, 1053–1123, 2005.

Odum, J. R., Hoffmann, T., Bowman, F., Collins, D., Flagan, R. C., and Seinfeld, J. H.: Gas/Particle partitioning and secondary organic aerosol yields, Environ. Sci. Technol., 30, 2580–2585, 1996.

Owen, S. M. Boissard, C., and Hewitt, C. N.: Volatile organic compounds (VOCs) emitted from 40 Mediterranean plant species: VOC speciation and extrapolation to habitat scale, Atmos. Environ., 35, 5393–5409, 2001.

Pankow, J. F.: An absorption model of gas/particle partitioning of organic compounds in the atmosphere, Atmos. Environ., 28, 185–188, 1994a.

Pankow, J. F., Seinfeld, J. H., Asher, W. E., and Erdakos, G. B.: Modelling the formation of secondary organic aerosol, 1. Application of theoretical principles to measurements obtained in the α-pinene/, β-

pinene/, sabinene/, d3-carene/, and cyclohexane/ ozone systems, Environ. Sci. Technol., 35, 1164–1172, 2001.

Pankow, J. F. and Asher, W. E.: SIMPOL.1: a simple group contribution method for predicting vapor pressures and enthalpies of vaporization of multifunctional organic compounds, Atmos. Chem. Phys., 8, 2773–2796, 2008.

Pankow, J. F.: Organic particulate material levels in the atmosphere: Conditions favoring sensitivity to varying relative humidity and temperature, PNAS., 107, 6682-6686, 2010.

Seinfeld, J. H., Erdakos, G. B., Asher, W. E., and Pankow, J. F.: Modelling the formation of secondary organic aerosol (SOA), 2. The predicted effects of relative humidity on aerosol formation in the alpha-pinene/, beta-pinene/, sabinene/, delta 3-carene/, and cyclohexane/ozone systems, Environ. Sci. Technol., 35, 1806–1817, 2001.

Seinfeld, J. H. and Pankow, J. F.: Organic atmospheric particulate material, Annu. Rev. Phys. Chem., 54, 121–140, 2003.

Wiedinmyer, C., Guenther, A., Harley, P., Hewitt, N., Geron, C., Artaxo, P., Steinbrecher, R., and Rasmussen, R.: Global Organic Emissions from Vegetation, in: Emissions of Atmospheric Trace Compounds, edited by: Granier, C., Artaxo, P., and Reeves, C., 544 pp., Kluwer Academic Publishers, Dordrecht, The Netherlands, 115–170, 2004.

Yu, J. Z., Flagan, R. C., and Seinfeld, J. H.: Identification of products containing –COOH, -OH, and –C=O in atmospheric oxidation of hydrocarbons, Environ. Sci. Technol., 32, 2357–2370, 1998.